Chemosphere 313 (2023) 137252

Contents lists available at ScienceDirect

Chemosphere

journal homepage: www.elsevier.com/locate/chemosphere

The chemical journey of Europium(III) through winter rye (*Secale cereale* L.) – Understanding through mass spectrometry and chemical microscopy

Julia Stadler [a,*], Manja Vogel [b,c], Robin Steudtner [d], Björn Drobot [d], Anna L. Kogiomtzidis [a], Martin Weiss [a], Clemens Walther [a]

[a] Institute of Radioecology and Radiation Protection, Leibniz University Hannover, 30419, Hannover, Germany
[b] VKTA – Strahlenschutz, Analytik & Entsorgung Rossendorf e.V., Bautzner Landstraße 400, 01328, Dresden, Germany
[c] HZDR Innovation GmbH, Bautzner Landstraße 400, 01328, Dresden, Germany
[d] Helmholtz-Zentrum Dresden-Rossendorf e.V., Institute of Resource Ecology, Bautzner Landstraße 400, 01328, Dresden, Germany

HIGHLIGHTS

- Spectroscopic, microscopic, and mass spectrometric methods were used to identify the journey of Eu(III) in *Secale cereale* L.
- Imaging of the plant part samples showed different distributions of Eu(III) species in the plant tissue.
- First possible Eu(III) species were identified in *Secale cereale* L. by ESI MS and TRLFS.

GRAPHICAL ABSTRACT

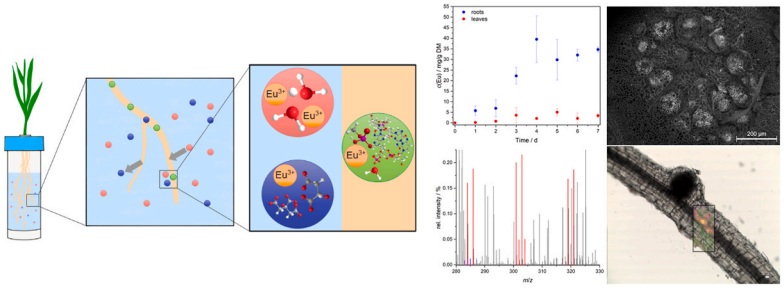

ARTICLE INFO

Handling Editor: Petra Petra Krystek

Keywords:
Rare earth elements
Plant uptake
Species analysis
Europium
Imaging

ABSTRACT

A combination of biochemical preparation methods with microscopic, spectroscopic, and mass spectrometric analysis techniques as contemplating state of the art application, was used for direct visualization, localization, and chemical identification of europium in plants. This works illustrates the chemical journey of europium (Eu (III)) through winter rye (*Secale cereale* L.), providing insight into the possibilities of speciation for Rare Earth Elements (REE) and trivalent f-elements. Kinetic experiments of contaminated plants show a maximum europium concentration in *Secale cereale* L. after four days. Transport of the element through the vascular bundle was confirmed with Scanning Electron Microscopy (SEM) and Energy Dispersive X-ray analysis (EDS). For chemical speciation, plants were grown in a liquid nutrition medium, whereby Eu(III) species distribution could be measured by mass spectrometry and luminescence measurements. Both techniques confirm the occurrence of Eu malate species in the nutrition medium, and further analysis of the plant was performed. Luminescence results indicate a change in Eu(III) species distribution from root tip to plant leaves. Microscopic analysis show at least three different Eu(III) species with potential binding to organic and inorganic phosphate groups and a Eu(III) protein complex. With plant root extraction, further europium species could be identified by using Electrospray Ionization Mass Spectrometry (ESI MS). Complexation with malate, citrate, a combined malate-citrate ligand, and aspartate was confirmed mostly in a 1:1 stoichiometry (Eu:ligand). The combination of the used analytical techniques opens new possibilities in direct species analysis, especially regarding to the understanding of rare

* Corresponding author.
E-mail address: stadler@irs.uni-hannover.de (J. Stadler).

https://doi.org/10.1016/j.chemosphere.2022.137252
Received 21 July 2022; Received in revised form 21 October 2022; Accepted 13 November 2022
Available online 17 November 2022

earth elements (REE) uptake in plants. This work provides a contribution in better understanding of plant mechanisms of the f-elements and their species uptake.

1. Introduction

In today's world, modern technology would be inconceivable without Rare Earth Elements (REEs). Fiber optics, flat screen displays, permanent magnets and auto catalysts are only a few examples (Gwenzi et al., 2018). In terms of the environmental impact, the REE concentrations in surrounding soil of mining sites or technological industries are verifiably increased compared to the amount present in the Earth's crust (Li et al., 2010). This is where plants can potentially take up the lanthanides from polluted soil and enter the human nutrition chain (Zhuang et al., 2017). Hazardous effects of high REE concentrations were investigated and further analyses are still in progress. Potential human health risks are well summarized by Gwenzi et al.: dysfunctional neurological disorders, cerium-pnemoconiosis, bone alteration, genotoxicity and fibrotic tissue injury, and anti-testicular effects (Gwenzi et al., 2018). In contrast, lower concentrations of REEs are commonly used as fertilizer in Chinese agriculture due to an enhancement in plant growth (Tyler, 2004). Various researches indicate a beneficial plant growth in presence of these elements and confirm their plant uptake (Buckingham et al., 1999; Pang et al., 2002; Tyler, 2004; Wang et al., 2000; Xu et al., 2002).

In the case of risk assessment, toxicity is strongly influenced by the elemental species due to differences in bioavailability (Ménétrier et al., 2008; Popplewell et al., 1991). An example is the variation in plant uptake of Europium (Eu(III)) from contaminated soils treated with different anionic ligands such as organic acids or phosphates (Jin et al., 2019; Zhimang et al., 2001). Bioaccessibility for the human body can also change with the variation of the chemical species present within the plant parts after ingestion. Differences in the absorption of metals and metal ions by animals have been shown to depend on their nature and species (Beyer et al., 2016; Li et al., 2017). In this context, research on the REEs behavior in plants and especially the species analysis are scarce, so a closer look into the plant uptake mechanism is crucial.

Europium as representative for the REEs is such an interesting candidate and few research has been published with its species analysis in plant parts (Fellows et al., 2003; Jessat et al., 2021; Moll et al., 2020). The outstanding properties of the element include the distinctive spectroscopic characteristics in its trivalent form and the presence of two stable isotopes ^{151}Eu and ^{153}Eu facilitating mass spectrometric identification. These properties are used to apply a wide variety of techniques for the analysis of Eu(III), such as luminescence spectroscopy or mass spectrometry (Heller et al., 2011; Sachs et al., 2015; Steppert et al., 2012; Stumpf et al., 2008). Fellows et al. investigated Eu(III) species in oat (*Avena sativa*) with laser-induced fluorescence spectroscopy indicating an accumulation of Eu(III) mainly in the meristematic cells located behind the root cap (Fellows et al., 2003). In this area, cell division rate and cell growth are relatively high. Additionally, during the growth of a plant, the Casparian band is expectably not fully developed, allowing metal ions to enter the xylem and distribution throughout the plant. Furthermore, a passive transport of Eu(III) via diffusion processes was assumed after detection of a high amount in the stele and maturation zone. Life-time measurements suggest inner-sphere Eu(III) mononuclear complexes inside the root, but the exact determination of the complex was not possible (Fellows et al., 2003). As plant membranes consist of functional groups of carbohydrates, proteins, and fats, these membrane constituents are most likely responsible for the transport of trivalent elements inside the cell (Ke and Rayson, 1993; Kelley et al., 1999; Texier et al., 2000). Eu(III) is proven to act as homologue for Ca (II) ions and for the trivalent actinides, e.g. Am(III) and Cm(III) due to their equal ionic radii and similarities in complex formation constants (Heller et al., 2011; Schmidt et al., 2009). In plants, transport via calcium channels was also investigated (Gao et al., 2003).

To improve the knowledge regarding Eu(III) uptake and its metabolism, this work focuses on the plant uptake in winter rye (*Secale cereal* L.), grown in a liquid nutrition medium. Analysis of the plant medium and direct analysis of the plant parts appear to be crucial for the chemical binding form (speciation) of Eu(III) (Alvares et al., 2007; Lourenco et al., 2006). Multiple techniques, e.g. luminescence spectroscopy, chemical microscopy and mass spectrometry were used for monitoring, quantifying and evaluating the transport pathway and speciation of Eu(III) within the plant.

2. Materials and methods

2.1. Chemicals

All solvents and reagents of analytical grade or higher were used without any purification. For dilution of reagents, MiliQ water (18.2 mΩ/cm) was used.

2.2. Plant growth

For the plant experiments, *Secale cereale* L. seeds (winter rye) were purchased from Bioland Hof Jeebel (Salzwedel, Germany). A scheme of the plant experiments that have been performed is shown in Fig. 1. First, the seeds were stored for 48–120 h in wet cellulose paper for germination. Afterwards, the seedlings were grown in a 1.5 L box with liquid nutrition medium, called Hoagland solution (Table 1), at pH 5.1 and $E_h = 570 \pm 60$ mV (Gupta et al., 2013). The Hoagland solution represents a chemical mixture of minerals typically present in environments with an optimal supply of nutrients for plant growth. Failure of growth or secondary processes started by survival mechanisms of the plants, i.e. deficiency diseases, can be excluded. To maintain controlled conditions for plant growth, the germ buds were stored for two weeks in a climatic chamber. A 18/6 h day/night cycle with a temperature of 22 ± 1/18 ± 1 °C and an illuminance of 120 µE/m^{2}s of a cold fluorescence lamp was chosen. The plants were grown under these conditions for a fortnight.

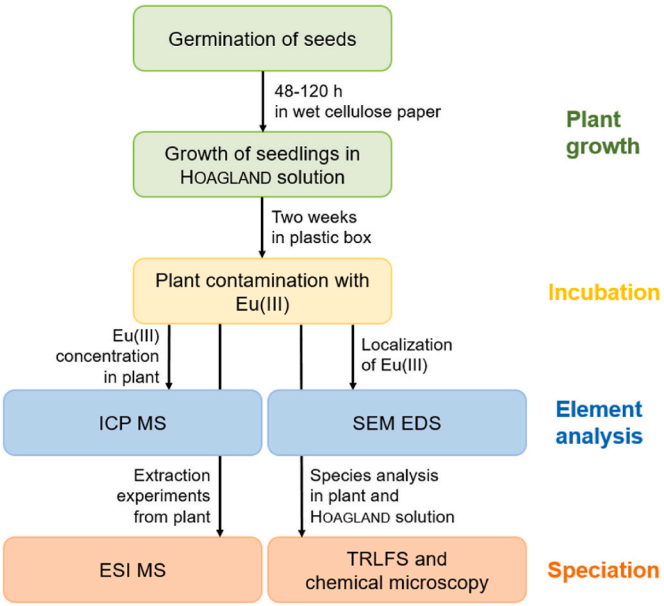

Fig. 1. Scheme of the plant experiments.

Table 1
Mineral content of Hoagland medium for plant growth of *Secale cereale* L.

Substance	Concentration/μM
KNO_3	1000
$Ca(NO_3)_2 \bullet 4H_2O$	300
$MgSO_4 \bullet 7H_2O$	200
$NH_4\ PO_4$	100
$FeSO_4 \bullet 7H_2O$	2
$Na_2EDTA \bullet 2H_2O$	1
H_3BO_3	5
$MnCl_2 \bullet 4H_2O$	1
$ZnSO_4 \bullet 7H_2O$	0.08
H_2MoO_4	0.06
$CuSO_4 \bullet 5H_2O$	0.03

For the contamination with Eu(III), a low-phosphate Hoagland medium ($[NH_4PO_4] = 25$ μM) was treated with europium(III) nitrate pentahydrate (99.9% trace metal basis, Sigma Aldrich). Therefore, plants were separated into two groups: one control group with the low-phosphate Hoagland solution, and one group with the Eu(III)-treated low--phosphate nutrition solution. The detection limits of the analytical techniques used for the species analysis were decisive for the europium concentration applied and therefore a concentration in the second group of [Eu(III)] = 5 mM ≈ 760 mg/L was chosen. With these conditions, a proof of principle of the used speciation methods could be done.

2.3. Mass spectrometric analysis of europium species

2.3.1. Determination of the europium concentration

The europium concentration inside the plant parts was determined by performing kinetic experiments over seven days. Two plant samples were harvested as control group at day zero. After plant growth and contamination with europium as described in section 2.2., three plants were sampled every day. The collected samples were prepared and analyzed separately. To obtain comparable results, plants of similar size were collected each day. Roots were washed to remove adsorbed europium from their surface and plants were separated into root and leaf parts by cutting above the root crown. Samples were dried for three days at 105 °C and dry weight was determined (Table S1). For the elemental characterization, plants were ashed and a microwave digestion with 3 M HNO_3 was performed. Afterwards, samples were evaporated to dryness, dissolved again in 2% HNO_3, and diluted for Inductively-Coupled Plasma Mass Spectrometer (ICP MS) measurements. The used device was a Thermo Fisher Scientific iCAPQ™ and was combined with a polytetrafluoroethylene nebulizer. A europium standard (plasma standard solution) purchased from Alfa Aesar (Kandel, Germany), nitric acid (69%) and methanol (HPLC grade) from VWR Chemicals (Langenfeld, Germany) were used. Evaluation was done by using DIN 38402 part 51 for calibration and DIN 32645 (2008) for calculation of the Limit of Detection (LOD) and Quantification (LOQ) (Deutsches Institut für Normung e.V., 2008, 2017). The results of europium concentration were normalized to the dry weight of the plant parts.

2.3.2. Plant extraction and species analysis

After evaluating the kinetic experiment above, plant roots were freshly separated after five days of plant contamination with 5 mM Eu (III). 40 mg sample material were frozen with liquid N_2 and milled for 60 s 200 μL of the extracting solution containing methanol and water (3:1) were added and milled again for 30 s. The last step was performed twice. Extract and residue were separated by centrifugation at 14 000 g. Afterwards, 10 μL of the extract were diluted to 100 μL by using the extracting solution. Samples were measured with an Electrospray Ionization Mass Spectrometer (ESI MS) consisting of a Nanospray Flex™ ion source and an Orbitrap Elite™ from Thermo Fisher Scientific. For analysis, 10 μL of each sample solution were transferred manually into a spray needle. For comparison, Eu(III) treated Hoagland media before and after contamination were also analyzed with ESI MS. Samples were diluted 1:10 with the same methanol water mixture (3:1) to achieve equal matrices. All measurements were performed in positive ion mode with a capillary temperature of 250 °C and a mass-to-charge range from m/z 100 to m/z 1000. Evaluation was performed with the software FreeStyle™ from Thermo Fisher Scientific and in-house-made program named MARI to identify isotopic pattern in Orbitrap™ spectra. The used program is described in the next chapter.

The ESI process causes additional water molecules to be attached to the measured species. They are generated by the droplet formation, which is depending on the instrument parameters (Beyer et al., 1999). For the used Orbitrap Elite™ the maximum number of water molecules that can attach to a compound during the ionization process was found to be three.

2.3.3. Identification of the isotopic pattern of europium in mass spectrometric spectra

For the isotopic pattern identification a new program was implemented, named MARI (*Mass spectra Analysis by Recognition of Isotopic pattern*). It consists of two self-developed algorithms to assist with the identification of europium compounds within the mass spectral data. The first one makes use of an element's characteristic isotope pattern to find all signals possibly caused by chemical species containing the element of interest. If a given element is present in multiple isotopic states A_1, …,A_N with masses m_1, …,m_N and abundances P_1, …,P_N, the isotopic pattern is defined by the mass differences $\Delta m_i = m_i - m_0$ and abundance ratios $\rho_i = P_i/P_0$ of the secondary isotopes A_i relative to the most abundant isotope A_0 (reference isotope). Assuming a charge state Z, the algorithm checks for every signal of the spectrum if the associated compound could contain the element's reference isotope by searching for the corresponding secondary isotope peaks. A signal (m/z_0, I_0) is treated as a result peak if for every secondary isotope A_i a matching signal (m/z_i, I_i) is found, for which the relative mass deviation in equation (1) and the relative abundance deviation in equation (2) lie within a user-defined tolerance range.

$$\delta m_i = \frac{m/z_i - m/z_0 - \Delta m_i/Z}{m/z_i} \quad (1)$$

$$\delta \rho_i = \frac{I_i/I_0 - \rho_i}{\rho_i} \quad (2)$$

The second algorithm compares the expected isotope peaks of a specific molecular compound with the experimental data. Based on an approach by Stoll et al., a score is calculated, which reflects how well the measurement data matches the expected peak distribution (Stoll et al., 2006). This score can give an indication as to whether the specified compound is present in the spectrum. For the relatively small metal complexes investigated in this study, the isotope pattern often is strongly dominated by the isotope distribution of the central metal atom. Therefore, minor isotopic peaks are of increased relevance to distinguish between different compounds. For this reason, two additional terms were included in the score calculation to enhance the impact of intensity deviations in minor isotopic peaks.

2.4. Localization of europium in Secale cereale L. root crown

Secale cereale L. was contaminated with [Eu(III)] = 10 mM in Hoagland medium and harvested after five days of contamination as described in the previous section 2.2. The root crown was cut into small slices of about 1 mm directly after harvesting, stuck on a carbon pad and mounted onto an aluminum sample holder. The cross section was measured with a SEM Philips XL30 ESEM and EDS from RemX GmbH. Analyses took place in low vacuum with a pressure of 1 mbar and an acceleration voltage of 30 kV. By using Scanning Electron Microscopy (SEM) and Energy-Dispersive X-ray Spectroscopy (EDS) europium was

localized inside the root crown. Subsequently, the cross section was scanned for further elements.

2.5. Eu(III) species distribution in Hoagland medium and Secale cereale L

2.5.1. Theoretical calculation

Theoretical pH diagram of the Eu(III) treated Hoagland solution ([Eu] = 5 mM, Table 1) was done with the program PhreePlot, based on PHREECQ calculations (Kinniburgh and Cooper, 2011, Last updated 2022; Parkhurst and Apello C.A.J.). Formation constants were taken from the ThermoChimie and Joint Expert Speciation System (JESS) databases (Table S2) (Giffaut et al., 2014; May et al., 2019; May and Murray, 1991).

2.5.2. Time-resolved laser-induced fluorescence spectroscopy measurements

Solutions were measured in 2 mL quartz glass cuvettes and plant parts in solid sample holders covered with quartz window using an excitation wavelength of 394 nm (Ekspla, NT230, ~5 ns pulse, 1.3 mJ/pulse). The temperature controlled cuvette holder was connected to the spectrograph (Andor, SR-303i-A, 300 L/mm, center wavelength 640 nm) via a light guide. Spectra were recorded with an ICCD (Andor iStar, DH320T-18U-63) using different parameter sets for liquid samples (50 µm input slit, gate width 0.2 ms, gain 1000) or solid samples (300 µm input slit, gate width 0.2 ms, gain 2000) respectively. Data deconvolution was performed with PARAFAC (N-way toolbox for Matlab (Andersson and Bro, 2000; Drobot et al., 2019)).

2.5.3. Chemical microscopy of Secale cereale L

Luminescence spectroscopic mapping of Eu(III) species in plant parts after incubation was carried out with a Raman microscope (LabRAM system, HORIBA Jobin Yvon, Lyon, France) for the spatial resolved excitation of the Eu(III) fluorescence using a 532 nm laser (Vogel et al., 2021). The fresh and optional razorblade cut samples were mounted on a glass objective slide with a drop of 0.1 M NaCl, covered by a cover slit and fixed on a piezo electrically driven microscope scanning stage. After an optional intensity filter, the laser beam was directed through an objective lens with 10fold or 50fold magnification onto the sample resulting in laser spot size of 2.6 µm and 0.9 µm, respectively. The analyzed sample areas were pinpointed by a camera. Eu(III) luminescence was collected in the wavelength range from 560 to 725 nm with the same objective lens and directed through a pinhole (200 µm) to a spectrometer (200 µm entrance slit, 300 gr/mm grating) that disperses the light before reaching the Peltier cooled CCD detector (−70 °C). Acquisition and basic treatment of data was performed with LabSpec 5 software (Horiba Jobin Yvon). All spectra were background corrected using a self-implemented version of a 'rolling ball' algorithm (Sternberg, 1982). Data deconvolution was performed by an iterative factor analysis (N-way toolbox for Matlab (Andersson and Bro, 2000)) using randomized initial guesses. The spectra of the factors and distributions were restricted to being non negative (NIFA – non-negative iterative factor analysis) (Vogel et al., 2021).

3. Results

3.1. Plant experiments and elemental content

Initially, over seven days of Eu(III) plant contamination, the plants were optically inspected and change in plant morphology is observed (Fig. 2a). The leaves seem a little browner as a consequence of europium uptake and transport into the leaves. In parallel, root and leaf parts were sampled for daily determination of the europium concentration in these plant parts by ICP MS (Fig. 2b). All values were calculated to be above the LOQ. For control plant parts on day zero, the europium concentrations were 0.016 ± 0.015 mg/g dry plant material (DM) for the roots and 0.0023 ± 0.00025 mg/g DM for the leaves. Up to the 4th day after contamination, the concentrations increased monotonously up to 2500-fold within the rye roots compared to day zero with 40 ± 11 mg/g DM. Thereafter, no further significant increase occurred. Similar behavior can be seen for the leaves, but with considerably less europium content of 5.1 ± 1.8 mg/g DM at day five (2200-fold of day zero). It appears that most of the europium is located in the roots and only a smaller amount is transported into the leaves. At day four and five the standard deviations of the europium concentration inside the roots are increased compared to days 0–3 and 6–7 and cannot be explained by systematic errors, such as differences in plant biomasses (Table S1). Elevated deviations have been shown to occur in plant uptake experiments and values of e.g. ± 70% have already been detected (Shtangeeva, 2014).

For the further experiments, an incubation period of five days was chosen for the plants, as the maximum europium concentration in roots and leaves together was already determined after five days.

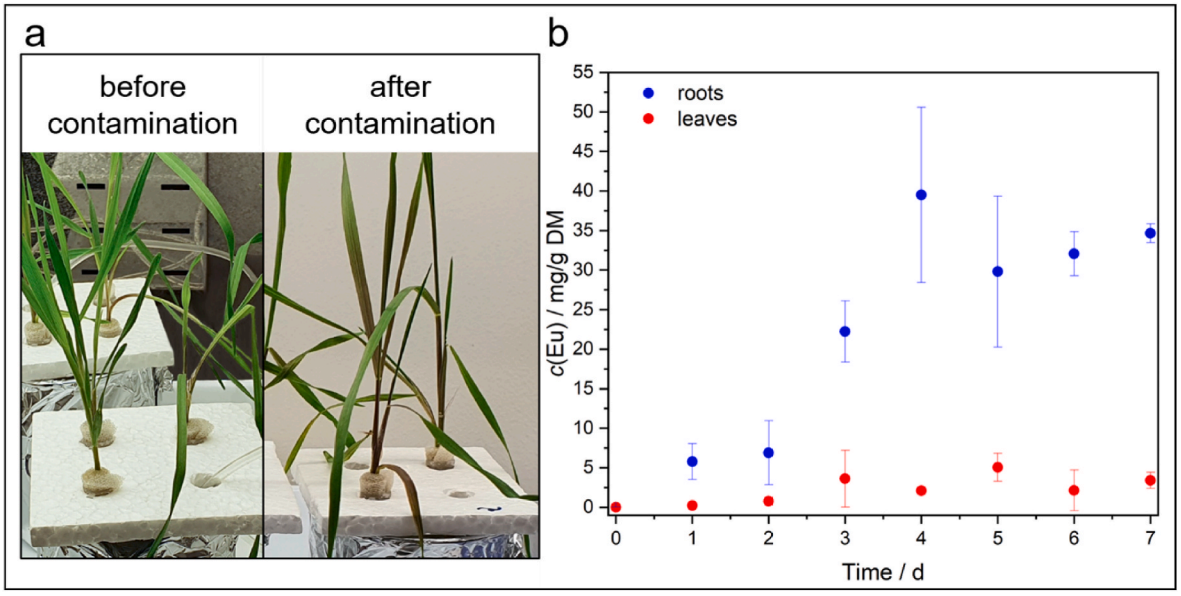

Fig. 2. (a) *Secale cereale* L. before and after contamination with 5 mM Eu(III). (b) Total europium content in *Secale cereale* L. roots and leaves within a contamination period of seven days. Contamination was carried out with a 5 mM Eu(III) Hoagland solution.

3.2. Localization of europium in Secale cereale L. root crown cross section

Localization of europium in *Secale cereale* L. root crown cross section and elemental composition in vascular bundles were measured by SEM EDS (Fig. 3). Utilization of the SEMS's low vacuum mode allows to measure intact plant material. Europium is identified through brighter spots in the transport channels of the cross section (Fig. 3a), confirming its transport from root via root crown to the leaves. EDS measurements of the bright areas clearly confirm the presence of europium due to the appearance of the respective X-ray lines. Europium seems to accumulate in transport channels, equal to e.g. Ca(II) and Fe(III) (Cataldo et al., 1988). Potassium, phosphorous, and sulfur X-ray lines are also present in the xylem proofing the mineral transport. Background signals are generated by carbon, oxygen, aluminum, and silicon and mainly originate from the sample holder. It might be surprising, that no Ca lines are visible in the EDS spectrum in (Fig. 3b), given that the Hoagland solution contains considerable amounts of Ca (Table 1). Interferences of close lying X-ray lines from potassium and calcium hinder an unambiguous evaluation.

3.3. Eu(III) speciation in Hoagland medium and Secale cereale L. by luminescence spectroscopy and microscopy

To understand the transport of the Eu(III) through an entire plant of *Secale cereale* L. we applied a combined multi-luminescence approach composed of classical Time-resolved Laser Fluorescence Spectroscopy (TRLFS) and chemical microscopy with high resolution emission spectra. For the determination of the chemical Eu(III) coordination sites we characterized the alteration of the Eu(III) species in the Hoagland solution and the plant parts directly by using a 394 nm laser system. This investigations were accompanied by an analysis of the spatial distribution of Eu(III) in different plant parts using microscopy with high resolution luminescence spectroscopy after excitation with 532 nm. In all measurements, the sensitive transitions of $^5D_0 \rightarrow {}^7F_0$ to $^5D_0 \rightarrow {}^7F_4$ were considered.

Initially, the emission spectra of the Eu(III) Hoagland medium were obtained before and during the plant contamination. Based on the PARAFAC analysis, two deconvoluted Eu(III) species with clear different spectral characteristics (Fig. 4c, Figure S1) were extracted for Eu(III) in the Hoagland solution over the incubation time of five days. Based on their spectral characteristic, presence of the $^5D_0 \rightarrow {}^7F_0$ transitions, their intensity ratios of the transitions $^5D_0 \rightarrow {}^7F_2$ and $^5D_0 \rightarrow {}^7F_1$ (F_2/F_1), and the luminescence lifetimes we assigned the blue Eu(III) species to the free Eu(III) aquo ion. The luminescence lifetime of 111 ± 1 μs and the F_2/F_1 ratio of 0.42 are well in agreement to literature data and this interpretation is supported by the theoretical thermodynamic speciation calculation of Eu(III) in Hoagland medium (Fig. 4a and b) (Bader et al., 2019).

The free Eu(III) aquo ion with 97.5 % is the dominant species up to pH 7. Minor contributors to the overall speciation, e.g. $Eu(SO_4)^+$ with 2.5 % were spectroscopically not visible. During incubation of the plant in Hoagland solution, a second species (orange) constantly occurred in the deconvoluted Eu(III) distribution (Fig. 4d) with a luminescence lifetime of 120 ± 1 μs, a F_2/F_1 ratio of 1.39 and an apparent $^5D_0 \rightarrow {}^7F_0$ transition. This orange species is attributed to an organic substance released by the winter rye root during incubation with Eu(III).

It is known that winter rye roots can secrete organic acids, e.g. malate and citrate (Li et al., 2000). Based on a comparison of the spectral features of the orange Eu(III) species with reference spectra of malate in sodium chloride and Hoagland solution a coordination by malate is most likely (Figure S2). Reference measurements of Eu(III)-malate in sodium chloride and Hoagland solution (Figure S1) revealed a prominent $^5D_0 \rightarrow {}^7F_0$ transition, luminescence lifetimes of 152 ± 1 μs and 135 ± 1 μs as well as a F_2/F_1 ratio of 1.49, respectively. The slight differences in spectral characteristics between the malate reference in sodium chloride and the malate reference as well as the orange species in Hoagland solution can be explained by interfering or quenching elements present in Hoagland solution (e.g. Fe) compared to sodium chloride as simpler background electrolyte (Tan et al., 2010).

Secondly, after two days incubation with 5 mM Eu(III) Hoagland solution, an entire plant was cut in twelve parts (Fig. 5a) which were then measured with TRLFS from the root to the leaves of *Secale cereale* L.

A global analysis of all plant parts data by PARAFAC revealed the existence of two distinct Eu(III) species (Fig. 5b) with clearly different spectral characteristics as the two Eu(III) species determined within the Hoagland medium. Immediately with association to *Secale cereale* L. a speciation change of Eu(III) occurred. As presented in Fig. 5c, the distribution of the analyzed Eu(III) species changes from roots to leaves. In the roots, the grey species dominates and in the lower leave parts (8–10) the brown species dominates. In general, the total Eu(III) luminescence intensity in the root samples was significantly higher compared to root crown and leaf parts (Fig. 5c). Independently of the detailed localization in the plant, all Eu(III) species assigned to *Secale cereale* L. show the $^5D_0 \rightarrow {}^7F_0$ transitions in their spectra and elevated F_2/F_1 ratios with 1.4 for the brown and 2.8 for the grey species compared to the ratio of 0.4 for the Eu(III) aquo ion (Fig. 5b). Furthermore, data analysis revealed two comparable lifetimes with 184 ± 6 μs and 240 ± 5 μs for the grey and brown species, respectively. As the species identified within the plant

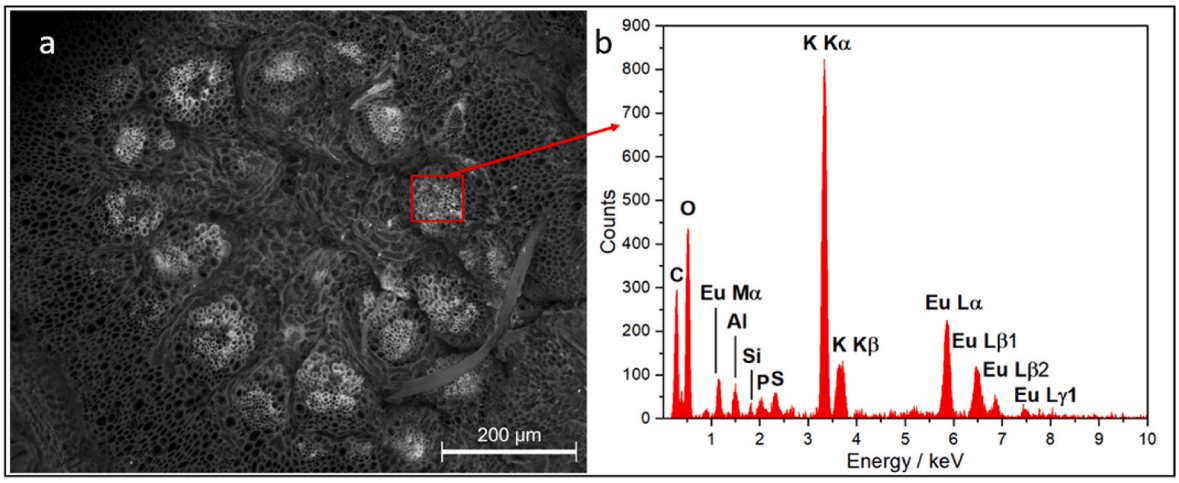

Fig. 3. *Secale cereale* L. root crown after contamination with europium in Hoagland solution, analyzed with SEM in back scattered electron mode (BSE) for localization of europium (a) and red marked area of EDS measurement for elemental identification (b). Brighter spots in BSE image were correlated to europium signals from EDS measurements. (For interpretation of the references to colour in this figure legend, the reader is referred to the Web version of this article.)

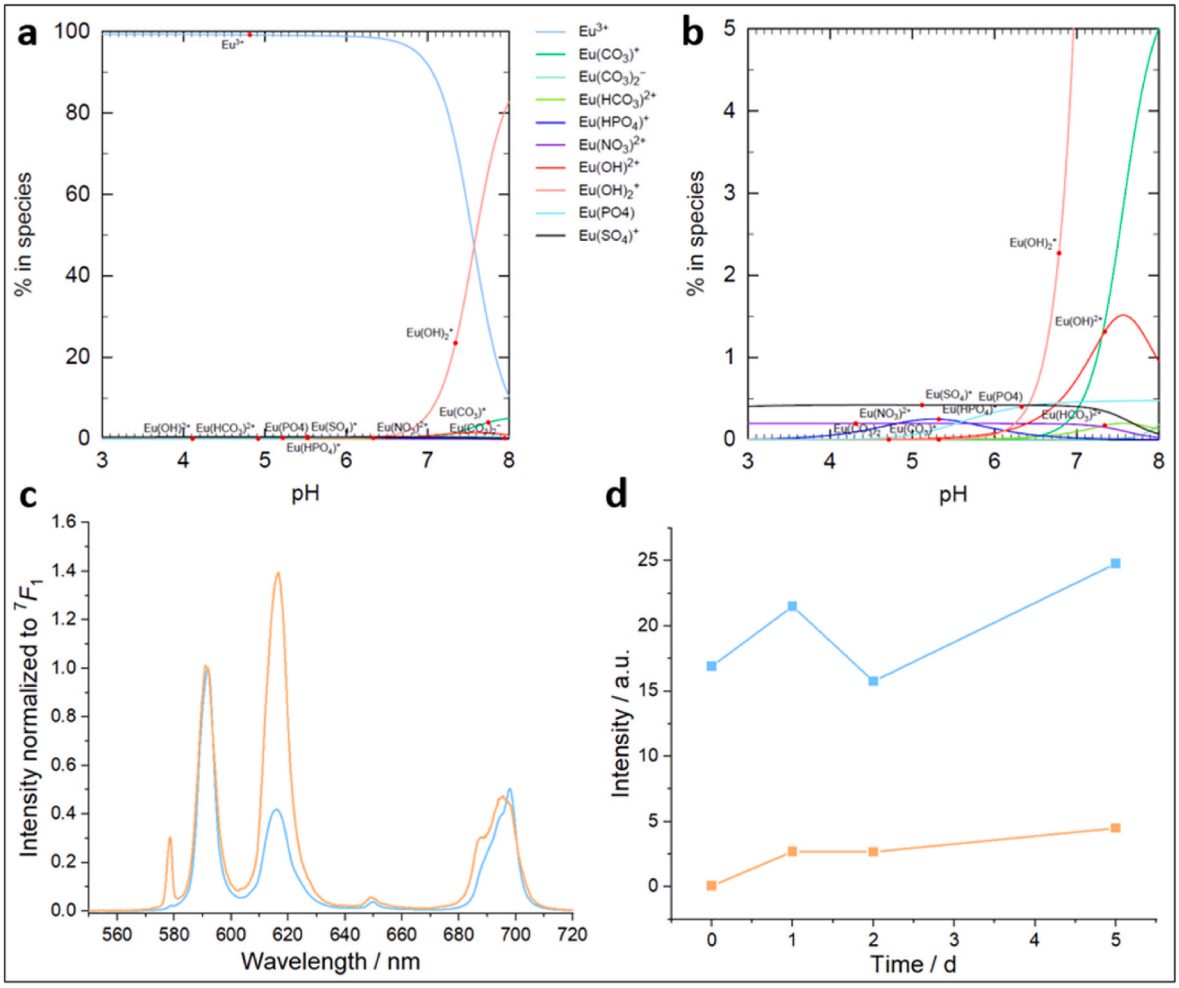

Fig. 4. (a) Theoretical thermodynamic speciation of Eu(III) in Hoagland medium calculated with PHREEQC using the ThermoChimie database. (b) Magnified section of graph (a). (c) Deconvoluted emission spectra of Eu(III) species in Hoagland solution assigned to Eu(III) aquo ion (blue) and Eu(III)-species 2 (orange) assigned to malate according to spectral features and luminescent life time. (d) Corresponding species distribution over incubation time of the two species. (For interpretation of the references to colour in this figure legend, the reader is referred to the Web version of this article.)

spectrally differ from free Eu(III) aquo ion and the Hoagland medium species it is likely that the species belong to Eu(III) complexes with plant tissue, organic acids or anions like phosphate. The relatively long lifetimes suggest tight complexation of Eu(III) to plant ligands and not only unspecific interactions to e.g. single carboxylic groups. However, TRLFS measurements of plant parts and corresponding data analysis turned out to be challenging due to the heterogeneity of the solid samples compared to solutions. Some plant parts are non-transparent and multiple scattering can occur. Therefore, in this study data analysis with PARAFAC was restricted and revealed only two species, which probably are a superposition of several species. To overcome the shortcomings of TRLFS measurements, a global analysis of the luminescence spectra obtained by chemical microscopy of selected plant parts of *Secale cereale* L. was carried out. Thin roots as well as cross sections of roots (root crown), and leaves were analyzed regarding the local distribution of Eu(III) species in plant tissue (Fig. 6). The spectral deconvolution of emission spectra from chemical microscopy using NIFA (Vogel et al., 2021) results in a spatially resolved image of chemical species as described in section 2.5.3. In the plant parts depicted in Fig. 6f, three Eu(III) species with different spectral features compared to the Eu(III) species in Hoagland medium are detected. So, the immediate speciation change between Hoagland solution and plant was also confirmed by this analysis.

The species identified by chemical microscopy show characteristic spectral features in all recorded $^5D_0 \rightarrow {}^7F_j$ transitions, which allows a clear local assignment within the plant. The F_2/F_1 ratio of 1.0 suggests a different symmetry in complexation of the Eu(III) ion by the magenta species compared to the yellow (F_2/F_1 ratio 3.7) and green (F_2/F_1 ratio 3.4) ones.

The magenta and yellow Eu(III) species are visible at the root tip (Fig. 6a), as well as strongly in the vascular bundle throughout the whole plant (Fig. 6b, d, e). It could be dissolved species, which are transported from roots via xylem sap to the leaves, or species formed after complexation with vascular tissue. The green Eu(III) species shows up mainly at the root tip/root cap meristem (Fig. 6a), in the cortex of the root (Fig. 6b), accompanied by the yellow Eu(III) species, and at the root hairs (Fig. 6c). As all three species show up at different plant parts it cannot be ruled out that more than one individual ligand is responsible for giving a certain binding motif. The spectral characteristics of the green species namely the prominent feature at the F_2 band and the chair-like shape of the F_4 band strongly suggest a binding of Eu(III) to organic phosphate groups. This hypothesis is supported by comparison of the green spectrum to spectra from literature for Eu(III) bound to phosphorylated compounds like DNA/RNA (Opherden et al., 2014; Vogel et al., 2021), phytic acid or phosphoenolpyruvate (Moll et al., 2021). The yellow species shows spectral similarities (F_2/F_1 ratio, shape of F_4 band) to protein bound Eu(III) (Calmodulin, α-Amylase) (Barkleit et al., 2016; Drobot et al., 2019), whereas the spectral features of the magenta species (small F_0, F_2/F_1 ratio, shape of F_4 band) point to an involvement of inorganic phosphate to Eu(III) coordination (compare Figure S3).

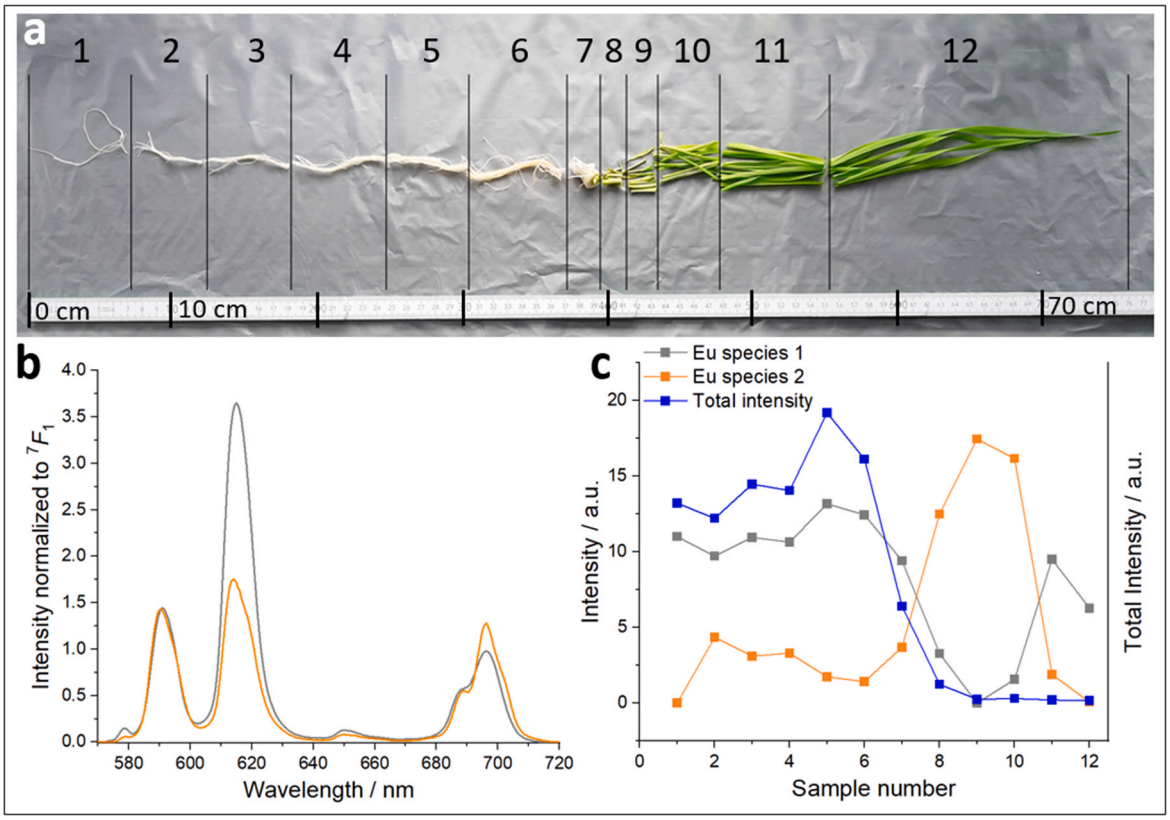

Fig. 5. Prepared *Secale cereale* L. plant used for luminescent measurements (a); PARAFAC deconvoluted TRLFS emission spectra of Eu(III) species in winter rye (b), corresponding species distribution from root tip (1) to leave tip (12) (c) and trend of total Eu(III) intensity within the entire plant.

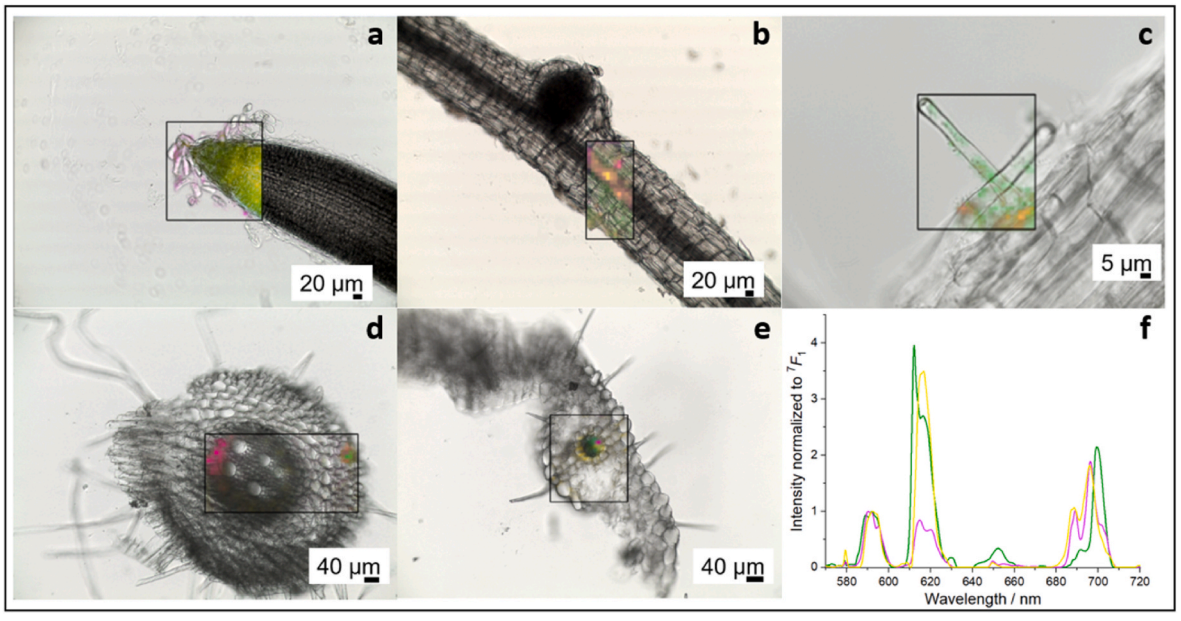

Fig. 6. Microscopic pictures of *Secale cereale* L. plant parts and overlaying Eu(III) species distribution within these parts. (a) Root tip; (b) thin root (no sectioning); (c) root hairs; (d) root cross section; (e) leaf cross section (f) PARAFAC deconvoluted chemical microscopy luminescence emission spectra of Eu(III) species in winter rye.

3.4. Plant extraction of europium species and mass spectrometric analysis

Extracts of *Secale cereale* L. roots as well as the europium Hoagland solution before and after treatment were analyzed with ESI MS to investigate the europium species content and its changes. By using the program MARI to identify the isotopic pattern of europium, several europium species were determined in the samples (Fig. 7, Table 2, Table S4). In the root extract, europium malate, citrate, a combined malate-citrate, and aspartate species were identified. To validate the existence and the formula of the found europium complexes, solutions with a concentration ratio of 1:1 ([Eu(III)]:[ligand]) were measured as references.

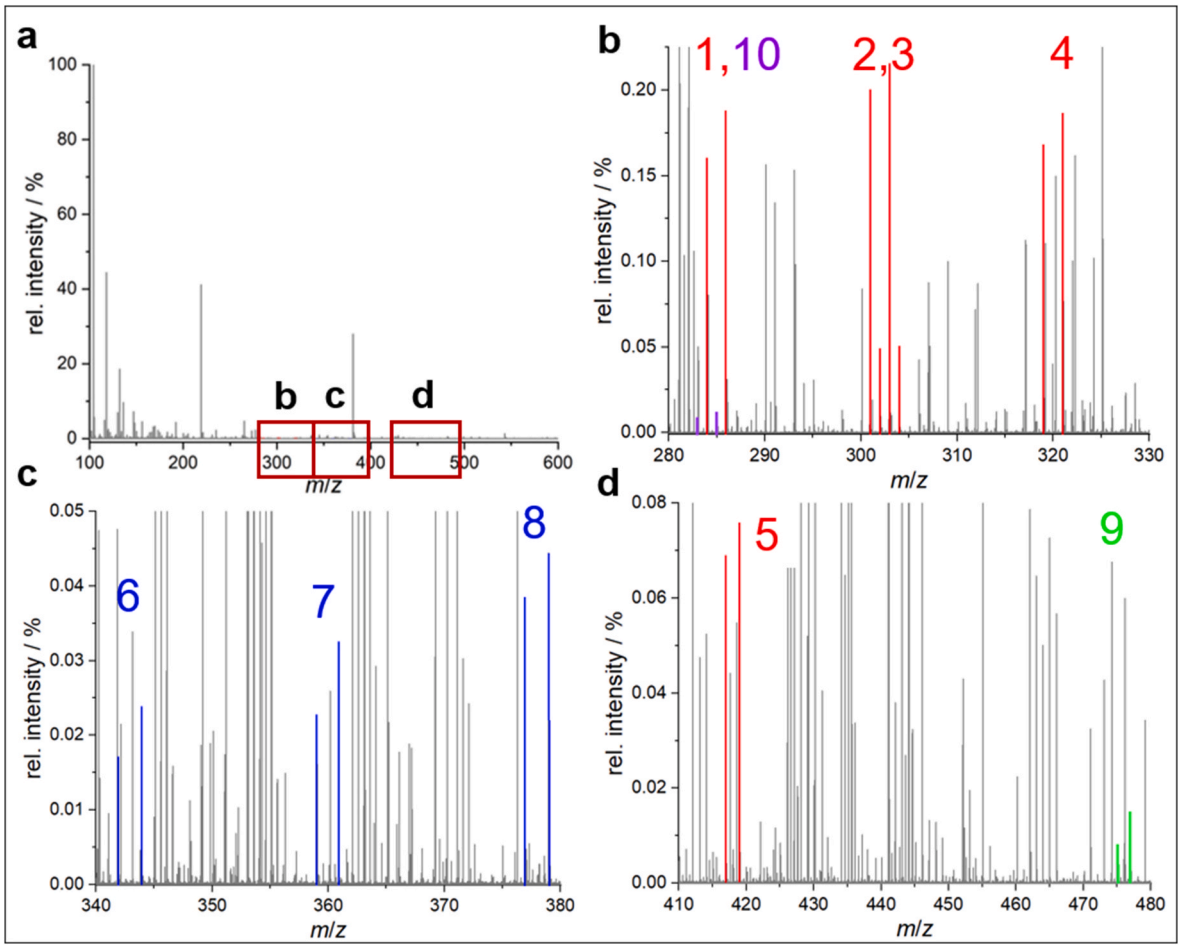

Fig. 7. ESI MS spectrum of the root extract of *Secale cereale* L. contaminated with 5 mM Eu(III) (a) with marked europium malate species in red (b, d), europium citrate in blue (c), a europium malate-citrate complex in green (d), and europium aspartate in violet (b) (Table 2) measured with 1.2 kV in positive ion mode. Grey signals are given by the background and plant metabolites. (For interpretation of the references to colour in this figure legend, the reader is referred to the Web version of this article.)

Table 2
Europium species (isotope ^{153}Eu) identified in *Secale cereale* L. root extract and europium Hoagland solution after plant contamination compared to europium reference solutions with malate , citrate, malate-citrate (, and aspartate ([Eu(III)]:[ligand] is 1:1 and [Eu(III)] = 0.1 mM) measured with ESI MS (Figure S6; Table S5-10). Relative intensities are given by the highest signal (100%) in each ESI MS spectrum

No.	Species	m/z[a] plant extract	rel. intensity/ %	m/z[a] Eu Hoagland after contamination	rel. intensity/ %	m/z[a] Eu reference solution	rel. intensity/ %
1	$[Eu(C_4H_5O_5)]^+$	285.934	1.73E-01	285.936	2.00E-02	285.932	2.07E-01
2	$[Eu(C_4H_4O_5) + H_2O]^+$	302.937	2.11E-01	302.937	9.78E-03	302.936	3.43E+01
3	$[Eu(C_4H_5O_5) + H_2O]^+$	303.945	4.95E-02	303.946	3.35E-04	303.947	1.22E-03
4	$[Eu(C_4H_5O_5) + 2H_2O]^+$	320.947	1.83E-01	320.948	5.77E-03	320.946	8.91
5	$[Eu(C_4H_5O_5)_2]^+$	418.948	6.88E-02	-	-	418.945	4.97
6	$[Eu(C_6H_6O_7) + H_2O]^+$	360.942	2.22E-02	-	-	360.941	1.20
7	$[Eu(C_6H_6O_7) + 2H_2O]^+$	378.953	4.48E-02	-	-	378.952	8.33E-01
8	$[Eu(C_6H_7O_7)]^+$	343.940	8.53E-03	-	-	343.939	8.25E-02
9	$[Eu(C_6H_7O_7)(C_4H_5O_4)]^+$	476.953	4.56E-03	-	-	476.954	1.19E+01
10	$[Eu(C_4H_5NO_4)]^+$	284.950	2.64E-03	-	-	284.948	2.51E-01

[a] m/z signal from ^{153}Eu; little variances are given by system calibration.

TRLFS measurements already indicated the presence of europium malate species in the Hoagland medium after plant contamination with Eu(III). In the plant root extract the complexes $[Eu(C_4H_5O_5)]^+$, $[Eu(C_4H_5O_5) + H_2O]^+$, $[Eu(C_4H_4O_5) + H_2O]^+$, and $[Eu(C_4H_4O_5) + 2H_2O]^+$ were identified by ESI MS. The extract shows one additional species $[Eu(C_4H_5O_5)_2]^+$. Their relative intensities were located from 0.2 to 0.007% related to the signal with the highest intensity in the mass spectrum. The identified species show divalent europium species frequently, which is an effect of charge transfer and hydrolysis during the ESI process (Beyer et al., 1999). However, identification of five different species could be obtained with ratios of 1:1 and 1:2 for europium to malate with up to two water molecules. In addition, europium citrate and a mixed species with citrate and malate were identified in the root extract with $[Eu(C_6H_6O_7) + H_2O]^+$, $[Eu(C_6H_6O_7) + 2H_2O]^+$, $[Eu(C_6H_7O_7)]^+$, and $[Eu(C_6H_7O_7)(C_4H_5O_4)]^+$ within the range of 0.04 to 0.009% relative intensity. Citrate and malate are assumed to be plant exudates, but no

europium citrate species were found in the Eu(III)-treated nutrition medium after plant contamination. This indicates a possible sorption of citrate species onto the plant root surface. Although the intensity of the ESI MS spectrum is lower than for the other species, a europium complex with the amino acid aspartate $[Eu(C_4H_5NO_4)]^+$ was identified, whereas it was not present in the Hoagland medium. Luminescence results confirm the absence of these europium species in the Hoagland medium, indicating their location inside the root of *Secale cereale* L.

4. Discussion

4.1. Elemental concentration in Secale cereale L

ICP MS and SEM EDS measurements proof the uptake of europium inside the roots and leaves of *Secale cereale* L. with decreasing concentration from roots to leaves. Only $\leq$25 % of the total amount of bound europium was detected inside the leaves. These results are in agreement with the initial Eu(III) analysis of the twelve separated plant parts measured by TRLFS. The decrease in Eu(III) concentration within the plant is not surprising and has already been determined by previous studies on the uptake of europium in plants (Shtangeeva, 2014; Shtangeeva and Ayrault, 2007). During transport of ions from the roots to the leaves in the non-living xylem vessels, important interactions take place between solutes and both the cell walls of the vessels and the surrounding xylem parenchyma cells. Major interactions are ion exchange adsorption of polyvalent cations in the cell walls, as well as uptake and release of elements and of organic solutes by surrounding living cells from xylem parenchyma and phloem. The retardation of cation transport thereby depends amongst others on the cation valence ($Ca^{2+} > K^+$) and whether the metal cations in the xylem are complexed to organic acids, amino acids or peptides (White, 2012).

Some plant experiments with europium uptake were performed during the second half of the 20th century indicating similar results. Shtangeeva and Zha et al. performed comparable experiments by using *Secale cereale* L. and a lower europium concentration of about 10 mg/kg in soil (Shtangeeva, 2014; Zha et al., 2014). The results showed a constantly increasing europium concentration inside the plant roots and leaves during the first ten days after contamination, with no maximum reached after few days. In a previous work with *Triticum aestivum*, the seedlings seem to accumulate a large amount of europium, depending on the stage of plant development (Shtangeeva and Ayrault, 2007). The authors suggested a europium release via water evaporation due to a decreasing concentration inside the plant and a decreasing amount in the rhizosphere. In our work, a maximum appears after only four days in the roots, which could be consistent with evaporation. Further accountable scenarios are europium accumulation up to a specific limit or an exchange with the nutrition medium until equilibrium is reached. Especially due to the usage of a liquid medium instead of soil the content of bioavailable minerals seems to be increased without complexing agents (Adeleke et al., 2017; Schaider et al., 2006). In addition, especially the soil composition is proven to influence uptake mechanisms due to a possible reduced bioavailability (Bunzl and Kracke, 1987; Kautenburger et al., 2017; Monsallier et al., 2003; Sokolik et al., 2004; Yang et al., 2014). Therefore, results obtained in this work are valid for the specified conditions of the plant contamination with europium.

4.2. Species analysis of europium within the plant

The initial analysis of Eu(III) in *Secale cereale* L. suggested a change in Eu(III) species within the plant parts from roots to leaves. Furthermore, microscopic analysis by using a Raman spectrometer gave more detailed information about the chemical environment of Eu(III). The occurrence of the green (Eu(III) organic phosphate) and the yellow species (Eu(III) protein) at the root cap and apical meristematic tissue can be easily explained with the presence of mucilaginous matrix, which mainly consists of proteins and polysaccharides and is responsible for root tip resistance to infections. Additionally, Wen et al. found that extracellular DNA (exDNA) is a component of root cap slime (Wen et al., 2009). Fellows et al.also reported about strong Eu(III) luminescence at the root tip of oat and explained that because of active cell division the ratio of DNA and protein to cell volume is very high in the apical meristematic region which favors a strong Eu(III) binding (Fellows et al., 2003). They further hypothesized that in the root tip area metal transport by diffusion to the xylem vessels is favored, as the Casparian stripes are not fully developed. As already mentioned above, polyvalent heavy metal ions, which are transported in the xylem sap, mainly exist in complexed form with organic acids, amino acids and peptides (White et al., 1981a, 1981b). The whole range of organic compounds are also found in phloem sap, for example secondary metabolites, hormones, proteins and RNA (Turgeon and Wolf, 2009). So the occurrence of the green and the yellow Eu(III) species (binding motif) in the vascular bundle throughout the whole plant and cortical tissue of the root is explainable. However, the exact ligand may have changed, e.g. DNA/RNA replaced by other organic phosphate.

The presence of Eu(III) complexed by inorganic phosphate (magenta species) at the root tip as well as in the vascular bundle seems reasonable as already very low amounts (~50 μM, Eu:PO_4 1:5) are sufficient to form clearly visible complexes with Eu(III) (compare Figure S3). For xylem sap with around 4 mM an appropriate phosphate content is reported in literature for *Brassica napus* L., *Nicotiana glauca* Grah. and *Ricinus communis* (Hocking, 1980; Nakamura et al., 2008; Schurr and Schulze, 1995).

Comparing these results with the obtained ESI MS analysis of the plant root extract, malate, citrate, and aspartate were identified as possible organic ligands for europium. For ESI MS several artifact formations were reported in previous researches (Beyer et al., 1999; Bush et al., 2008; Hester et al., 2016; Lightcap et al., 2016). An important formation for this work is the charge transfer reaction of the central metal ion, which can cause a notional divalent charge of europium (Bush et al., 2008). Considering these circumstances and the redox behavior of europium, the identified Eu(II) species are most likely to be present as Eu (III). Going further with the classification of the found europium ligands, the organic acids malate and citrate play important roles in the TriCarboxylic Acid cycle (TCA) taking place in the plant mitochondria. Citrate is a precursor of the TCA cycle, which is also called the citrate cycle. Moreover, citrate as a plant exudate is thought to support metal residency by complexing potentially hazardous metal ions or contribute to acidification of the surrounding soil to dissolve essential metal ions (Osmolovskaya et al., 2018). Malate, in addition to its function as an intermediate carboxylic acid, is also involved in carbon accumulation during the day for nocturnal plant respiration .(Korla and Mitra, 2014)

The third identified ligand aspartate is a precursor for several amino acids and is involved in the gluconeogenesis of the plant (Schulze et al., 2002). Furthermore, the formation of europium aspartate indicates the Eu(III) protein complex postulated in microscopic analysis. The aspartate malate shuttle gives a correlation to malate and makes its appearance more likely. It represents an indirect energy transfer into the plant mitochondria. Malate is transported across the mitochondrial membrane in exchange for α-ketoglutarate to synthesize NADH from NAD^+ and the malate, converted by the malate dehydrogenase. This reaction forms oxaloacetate, which has to be transformed into α-ketoglutarate to pass the membrane again. A transamination reaction takes place with glutamate forming aspartate. An involvement of europium could prevent this process by complex formation with malate and/or aspartate (Beeckams and Kanarek, 1981).

With luminescence spectroscopy and microscopy measurements inside the plant root, different Eu(III) species were postulated. Due to the presence of europium malate species in the root extract and the Hoagland solution after plant contamination, a sorption of these complexes on root hairs, or an exudation of malate bound to europium cannot be ruled out (Li et al., 2000; Osmolovskaya et al., 2018). An uptake of formed europium malate after exudation from *Secale cereale* L. seems to

be possible as well. Differences in postulated species can also be explained by the diverse characteristics of the analytical techniques applied: The intensity of europium malate inside the plant might be relatively low, which can be changed by extraction. This results in an accumulation of the species preferred by the solubility of the used extracting solvent. In the luminescence spectra from the plant root, the species might be present in the background but due to extraction, they were separated from the rest and readily identified in the ESI MS spectrum. Finally, in the plant itself not only one ligand seems to be involved in europium uptake mechanism. Dissolved and more complex europium species are presumably be formed. Thus, the metal ion can interact with different plant components and might perturb plant metabolism such as mitochondrial processes, e.g. the energy production. The results demonstrate the complexity and furthermore the necessity of species analysis inside the plant parts.

5. Conclusion

A first overview of elemental and species behavior of europium in *Secale cereale* L. and the nutrition medium was given in this work. Analysis of the Eu(III)-treated Hoagland solution suggest the formation of europium malate after plant contamination with luminescence and mass spectrometric measurements. Transport of europium across the vascular bundle into the leaves was confirmed by the use of ICP MS, SEM EDS and chemical microscopy. Kinetic experiments indicated a maximum uptake of europium after four days of plant contamination. With extraction experiments, europium complexation with the organic ligands malate, citrate, a combined malate-citrate, and aspartate were identified in the plant roots or adsorbed on the root surface. The identified ligands play important roles in the plant metabolism, especially in energy production via TCA cycle or transport mechanisms, e.g. the aspartate malate shuttle (Beeckams and Kanarek, 1981; Schulze et al., 2002). Many of the mentioned mechanisms are present in the mitochondria, indicating an active uptake of europium into the plant cells or a transport across the cell walls. Having a closer look into the plant's inside by using chemical microscopy, three Eu(III) species in different compartments of the *Secale cereale* L. were calculated using iterative factor analysis. Changes in Eu(III) species and their localization across the whole plant have been shown. The formation of inorganic phosphate, proteins, and an organic phosphorylated complex such as DNA/RNA with Eu(III) are assumed.

In general, luminescence measurements, microscopic and mass spectrometric analysis is shown to be a promising combination for species analysis of REE in biological samples. First identified species were obtained, contributing to a step forward in achieving a better understanding in plant uptake mechanisms and in bioavailability of REE with regard to human digestion and risk assessment.

Author contribution statement

Julia Stadler: Conceptualization, Methodology, Validation, Formal analysis, Investigation, Writing – original draft, Visualization **Manja Vogel:** Methodology, Formal analysis, Investigation, Writing – original draft, Visualization **Robin Steudtner:** Formal analysis, Investigation, Writing – review & editing, Visualization **Björn Drobot:** Software, Formal analysis, Writing – review & editing, Visualization **Anna L. Kogiomtzidis:** Software, Writing – review & editing **Martin Weiss:** Methodology, Investigation, Writing – review & editing **Clemens Walther:** Resources, Writing – review & editing, Supervision, Funding acquisition.

Declaration of competing interest

The authors declare that they have no known competing financial interests or personal relationships that could have appeared to influence the work reported in this paper.

Data availability

Data will be made available on request.

Acknowledgements

We would like to thank the Siebold-Sasse-Foundation for financial support.

Appendix A. Supplementary data

Supplementary data to this article can be found online at https://doi.org/10.1016/j.chemosphere.2022.137252.

References

Adeleke, R., Nwangburuka, C., Oboirien, B., 2017. Origins, roles and fate of organic acids in soils: a review. South Afr. J. Bot. 108, 393–406. https://doi.org/10.1016/j.sajb.2016.09.002.

Alvares, R., Bryan, N.D., May, I. (Eds.), 2007. Recent Advances in Actinide Science. Royal Society of Chemistry, Cambridge. https://dx.doi.org/10.1039/9781847555366-00001.

Andersson, G.A., Bro, R., 2000. The N-way toolbox for MATLAB. Chemometr. Intell. Lab. Syst. 52, 1–4. https://doi.org/10.1016/S0169-7439(00)00071-X.

Bader, M., Moll, H., Steudtner, R., Lösch, H., Drobot, B., Stumpf, T., Cherkouk, A., 2019. Association of Eu(III) and Cm(III) onto an extremely halophilic archaeon. Environ. Sci. Pollut. Res. Int. 26 (9), 9352–9364. https://doi.org/10.1007/s11356-019-04165-7.

Barkleit, A., Heller, A., Ikeda-Ohno, A., Bernhard, G., 2016. Interaction of europium and curium with alpha-amylase. Dalton Trans. 45 (21), 8724–8733. https://doi.org/10.1039/c5dt04790k.

Beeckams, S., Kanarek, L., 1981. Demonstration of physical interactions between consecutive enzymes of the citric acid cycle and of the aspartate-malate shuttle. Eur. J. Biochem. 117, 527–535. https://doi.org/10.1111/j.1432-1033.1981.tb06369.x.

Beyer, M., Williams, E.R., Bondybey, V.E., 1999. Unimolecular reactions of dihydrated alkaline earth metal discations $M^{2+}(H_2O)_2$, M = Be, Mg, Ca, Sr, and Ba: salt-bridge mechanism in the proton-transfer reaction $M^{2+}(H_2O)_2 \rightarrow MOH^+ + H3O^+$. J. Am. Chem. Soc. 121 (7), 1565–1573. https://doi.org/10.1021/ja982653+.

Beyer, W.N., Basta, N.T., Chaney, R.L., Henry, P.F.P., Mosby, D.E., Rattner, B.A., Scheckel, K.G., Sprague, D.T., Weber, J.S., 2016. Bioaccessibility tests accurately estimate bioavailability of lead to quail. Environ. Toxicol. Chem. 35 (9), 2311–2319. https://doi.org/10.1002/etc.3399.

Buckingham, S., Maheswaran, J., Meehan, B., Peverill, K., 1999. The role of applications of rare earth elements in enhancement of crop and pasture production. Mater. Sci. Forum 315–317, 339–347. https://dx.doi.org/10.4028/www.scientific.net/MSF.315-317.339.

Bunzl, K., Kracke, W., 1987. Soil to plant transfer of $^{239+240}$Pu, ^{238}Pu, ^{241}Am, ^{137}Cs and ^{90}Sr from global fallout in flour and bran from wheat, rye, barley and oats, as obtained by field measurements. The Science of Total Enivornment 63, 111–124. https://doi.org/10.1016/0048-9697(87)90040-4.

Bush, M.F., Saykally, R.J., Williams, E.R., 2008. Reactivity and infrared spectroscopy of gaseous hydrated trivalent metal ions. J. Am. Chem. Soc. 130 (28), 9122–9128. https://doi.org/10.1021/ja801894d.

Cataldo, D.A., McFadden, K.M., Garland, T.R., Wildung, R.E., 1988. Organic constituents and complexation of nickel(II), iron(III), cadmium(II) and plutonium(IV) in soybean xylem exudates. Plant Physiol. 86, 734–739. https://doi.org/10.1104/pp.86.3.734.

Deutsches Institut für Normung e.V., 2008. Chemische Analytik - Nachweis-, Erfassungs- und Bestimmungsgrenze unter Wiederholbedingungen - Begriffe, Verfahren, Auswertung. Beuth Verlag GmbH, Berlin, p. 28, 71.040.01.

Deutsches Institut für Normung e.V., 2017. Deutsche Einheitsverfahren zur Wasser-, Abwasser- und Schlammuntersuchung - Allgemeine Angaben (Gruppe A) - Teil 51: Kalibrierung von Analysenverfahren - Lineare Kalibrierfunktion (A 51). Beuth Verlag GmbH, Berlin, p. 16, 13.060.50.

Drobot, B., Schmidt, M., Mochizuki, Y., Abe, T., Okuwaki, K., Brulfert, F., Falke, S., Samsonov, S.A., Komeiji, Y., Betzel, C., Stumpf, T., Raff, J., Tsushima, S., 2019. Cm^{3+}/Eu^{3+} induced structural, mechanistic and functional implications for calmodulin. Phys. Chem. Chem. Phys. 21 (38), 21213–21222. https://doi.org/10.1039/c9cp03750k.

Fellows, R.J., Wang, Z., Ainsworth, C.C., 2003. Europium uptake and partitioning in oat (*Avena sativa*) roots as studied by laser-induced fluorescence spectroscopy and confocal microscopy profiling technique. Environ. Sci. Technol. 37 (22), 5247–5253. https://doi.org/10.1021/es0343609.

Gao, Y., Zeng, F., an Yi, Ping, S., Jing, L., 2003. Research of the entry of eare earth elements Eu^{3+} and La^{3+} into plant cell. Biol. Trace Elem. Res. 91, 253–265. https://doi.org/10.1385/BTER:91:3:253.

Giffaut, E., Grivé, M., Blanc, P., Vieillard, P., Colàs, E., Gailhanou, H., Gaboreau, S., Marty, N., Madé, B., Duro, L., 2014. Andra thermodynamic database for performance assessment: ThermoChimie. Appl. Geochem. 49, 225–236. https://doi.org/10.1016/j.apgeochem.2014.05.007.

Gupta, D.K., Inouhe, M., Rodríguez-Serrano, M., Romero-Puertas, M.C., Sandalio, L.M., 2013. Oxidative stress and arsenic toxicity: role of NADPH oxidases. Chemosphere 90 (6), 1987–1996. https://doi.org/10.1016/j.chemosphere.2012.10.066.

Gwenzi, W., Mangori, L., Danha, C., Chaukura, N., Dunjana, N., Sanganyado, E., 2018. Sources, behaviour, and environmental and human health risks of high-technology rare earth elements as emerging contaminants. The Science of Total Enivornment 636, 299–313. https://doi.org/10.1016/j.scitotenv.2018.04.235.

Heller, A., Barkleit, A., Bernhard, G., 2011. Chemical speciation of trivalent actinides and lanthanides in biological fluids: the dominant in vitro binding form of curium(III) and europium(III) in human urine. Chem. Res. Toxicol. 24 (2), 193–203. https://doi.org/10.1021/tx100273g.

Hester, T.H., Albury, R.M., Pruitt, C.J.M., Goebbert, D.J., 2016. Fragmentation of [Ni$(NO_3)_3$]$^-$: a study of nickel-oxygen bonding and oxidation states in nickel oxide fragments. Inorg. Chem. 55 (13), 6634–6642. https://doi.org/10.1021/acs.inorgchem.6b00812.

Hocking, P.J., 1980. The composition of phloem exudate and xylem sap from tree tobacco (*Nicotiana glauca* Grah.). Ann. Bot. 45 (6), 633–643. https://doi.org/10.1093/oxfordjournals.aob.a085871.

Jessat, J., Sachs, S., Moll, H., John, W., Steudtner, R., Hübner, R., Bok, F., Stumpf, T., 2021. Bioassociation of U(VI) and Eu(III) by plant (*Brassica napus*) suspension cell cultures-A spectroscopic investigation. Environ. Sci. Technol. 55 (10), 6718–6728. https://doi.org/10.1021/acs.est.0c05881.

Jin, S., Hu, Z., Huang, Y., Hu, Y., Pan, H., 2019. Evaluation of several phosphate amendments on rare earth element concentrations in rice plant and soil solution by X-ray diffraction. Chemosphere 236, 124322. https://doi.org/10.1016/j.chemosphere.2019.07.053.

Kautenburger, R., Sander, J.M., Hein, C., 2017. Europium (III) and Uranium (VI) complexation by natural organic matter (NOM): effect of source. Electrophoresis 38 (6), 930–937. https://doi.org/10.1002/elps.201600488.

Ke, H.-Y.D., Rayson, G.D., 1993. Luminescence Study of Eu^{3+} Binding to Immobilized *Datura innoxia* Biomaterial 27, 2466–2471. https://doi.org/10.1021/es00048a024.

Kelley, C., Mielke, R.E., Dimaquibo, D., Curtis, A.J., DeWitt, J.G., 1999. Adsorption of Eu (III) onto roots of water hyacinth. Environ. Sci. Technol. 33 (9), 1439–1443. https://doi.org/10.1021/es9807789.

Kinniburgh, D.G., Cooper, D.M., 2011. Last Updated 2022. PhreePlot: Creating Graphical Output with PHREEQC. Available at: http://www.phreeplot.org/.

Li, X.F., Ma, J.F., Matsumoto, H., 2000. Pattern of aluminum-induced secretion of organic acids differs between rye and wheat. Plant Physiol. 123, 1537–1543. https://doi.org/10.1104/pp.123.4.1537.

Korla, K., Mitra, C.K., 2014. Modelling the Krebs cycle and oxidative phosphorylation. Journal of Biomolecular Structure & Dynamics 32 (2), 242–256. https://doi.org/10.1080/07391102.2012.762723.

Li, J., Hong, M., Yin, X., Liu, J., 2010. Effects of the accumulation of the rare earth elements on soil macrofauna community. J. Rare Earths 28 (6), 957–964. https://doi.org/10.1016/S1002-0721(09)60233-7.

Li, H.-B., Li, J., Zhao, Di, Li, C., Wang, X.-J., Sun, H.-J., Juhasz, A.L., Ma, L.Q., 2017. Arsenic relative bioavailability in rice using a mouse arsenic urinary excretion bioassay and its application to assess human health risk. Environ. Sci. Technol. 51 (8), 4689–4696. https://doi.org/10.1021/acs.est.7b00495.

Lightcap, J., Hester, T.H., Kamena, K., Albury, R.M., Pruitt, C.J.M., Goebbert, D.J., 2016. Gas-phase fragmentation of aluminum oxide nitrate anions driven by reactive oxygen radical ligands. J. Phys. Chem. A 120 (9), 1501–1507. https://doi.org/10.1021/acs.jpca.5b12417.

Lourenco, V., Ansoborlo, E., Cote, G., Moulin, C., 2006. Speciation of radionuclides with bioligands using time-resolved laser-induced fluorescence (TRLIF) and electrospray mass spectrometry (ES-MS).

May, P.M., Murray, K., 1991. JESS, A joint expert speciation system—I. Raison d'être. Talanta 38 (12), 1409–1417. https://doi.org/10.1016/0039-9140(91)80289-C.

May, P.M., Rowland, D., Murray, K., 2019. Joint expert speciation system - JESS primer. Available at: http://jess.murdoch.edu.au/jess_home.htm.

Ménétrier, F., Taylor, D.M., Comte, A., 2008. The biokinetics and radiotoxicology of curium: a comparison with americium. Appl. Radiat. Isot. 66 (5), 632–647. https://doi.org/10.1016/j.apradiso.2007.12.002.

Moll, H., Sachs, S., Geipel, G., 2020. Plant cell (*Brassica napus*) response to europium(III) and uranium(VI) exposure. Environ. Sci. Pollut. Res. Int. 27 (25), 32048–32061. https://doi.org/10.1007/s11356-020-09525-2.

Moll, H., Barkleit, A., Frost, L., Raff, J., 2021. Curium(III) speciation in the presence of microbial cell wall components. Ecotoxicol. Environ. Saf. 227, 112887 https://doi.org/10.1016/j.ecoenv.2021.112887.

Monsallier, J.-M., Artinger, R., Denecke, M.A., Scherbaum, F.J., Buchau, G., Kim, J.-I., 2003. Spectroscopic study (TRLFS and EXAFS) of the kinetics of An(III)/Ln(III) humate interaction. Radiochim. Acta 91, 567–574. https://doi.org/10.1524/ract.91.10.567.22471.

Nakamura, S., Akiyama, C., Sasaki, T., Hattori, H., Chino, M., 2008. Effect of cadmium on the chemical composition of xylem exudate from oilseed rape plants (*Brassica napus* L.). Soil Sci. Plant Nutr. 54 (1), 118–127. https://doi.org/10.1111/j.1747-0765.2007.00214.x.

Opherden, L., Oertel, J., Barkleit, A., Fahmy, K., Keller, A., 2014. Paramagnetic decoration of DNA origami nanostructures by Eu^{3+} coordination. Langmuir 30 (27), 8152–8159. https://doi.org/10.1021/la501112a.

Osmolovskaya, N., Viet Vu, D., Kuchaeva, L., 2018. The role of organic acids in heavy metal tolerance in plants. Biological Communications 63 (1), 9–16. https://doi.org/10.21638/spbu03.2018.103.

Pang, X., Li, D., Peng, an, 2002. Application of rare-earth elements in the agriculture of China and its environmental behavior in soil. Environ. Sci. Pollut. Res. Int. 9 (2), 143–148. https://doi.org/10.1007/BF02987462.

Parkhurst, D.L., Apello C.A.J. Description of input for PHREEQC version 3—a computer program for speciation, batch-reaction, one-dimensional transport, and inverse geochemical calculations. U.S. Geological Survey Techniques and Methods. book 6, chap. A43, 497 p. doi:10.3133/tm6A43.

Popplewell, D.S., Harrison, J.D., Ham, G.J., 1991. Gastrointestinal absorption of neptunium and curium in humans. Health Phys. 60 (6), 797–805. https://doi.org/10.1097/00004032-199106000-00005.

Sachs, S., Heller, A., Weiss, S., Bok, F., Bernhard, G., 2015. Interaction of Eu(III) with mammalian cells: cytotoxicity, uptake, and speciation as a function of Eu(III) concentration and nutrient composition. Toxicol. Vitro 29 (7), 1555–1568. https://doi.org/10.1016/j.tiv.2015.06.006.

Schaider, L.A., Parker, D.R., Sedlak, D.L., 2006. Uptake of EDTA-complexed Pb, Cd and Fe by solution- and sand-cultured *Brassica juncea*. Plant Soil 286 (1–2), 377–391. https://doi.org/10.1007/s11104-006-9049-8.

Schmidt, M., Stumpf, T., Walther, C., Geckeis, H., Fanghänel, T., 2009. Incorporation versus adsorption: substitution of Ca^{2+} by Eu^{3+} and Cm^{3+} in aragonite and gypsum. Dalton Trans. 33, 6645–6650. https://doi.org/10.1039/b822656c.

Schulze, J., Tesfaye, M., Litjens, R.H.M.G., Bucciarelli, B., Trepp, G., Miller, S., Samac, D., Allan, D., Vance, C.P., 2002. Malate plays a central role in plant nutrition. Plant Soil 247, 133–139. https://doi.org/10.1007/978-94-017-2789-1_10.

Schurr, U., Schulze, E.-D., 1995. The concentration of xylem sap constituents in root exudate, and in sap from intact, transpiring castor bean plants (*Ricinus communis* L.). Plant Cell Environ. 18 (4), 409–420. https://doi.org/10.1111/j.1365-3040.1995.tb00375.x.

Shtangeeva, I., 2014. Europium and cerium accumulation in wheat and rye seedlings. Water, Air, Soil Pollut. 225 (6) https://doi.org/10.1007/s11270-014-1964-3.

Shtangeeva, I., Ayrault, S., 2007. Effects of Eu and Ca on yield and mineral nutrition of wheat (*Triticum aestivum*) seedlings. Environ. Exp. Bot. 59 (1), 49–58. https://doi.org/10.1016/j.envexpbot.2005.10.011.

Sokolik, G.A., Ovsiannikova, S.V., Ivanova, T.G., Leinova, S.L., 2004. Soil-plant transfer of plutonium and americium in contaminated regions of Belarus after the Chernobyl catastrophe. Environ. Int. 30 (7), 939–947. https://doi.org/10.1016/j.envint.2004.03.003.

Steppert, M., Císařová, I., Fanghänel, T., Geist, A., Lindqvist-Reis, P., Panak, P., Štěpnička, P., Trumm, S., Walther, C., 2012. Complexation of europium(III) by bis(dialkyltriazinyl)bipyridines in 1-octanol. Inorg. Chem. 51 (1), 591–600. https://doi.org/10.1021/ic202119x.

Sternberg, S.R., 1982. Cellular Computers and Biomedical Image Processing. Springer, Berlin, Heidelberg.

Stoll, N., Schmidt, E., Thurow, K., 2006. Isotope pattern evaluation for the reduction of elemental compositions assigned to high-resolution mass spectral data from electrospray ionization Fourier transform ion cyclotron resonance mass spectrometry. J. Am. Soc. Mass Spectrom. 17 (12), 1692–1699. https://doi.org/10.1016/j.jasms.2006.07.022.

Stumpf, S., Stumpf, T., Lützenkirchen, J., Walther, C., Fanghänel, T., 2008. Immobilization of trivalent actinides by sorption onto quartz and incorporation into siliceous bulk: investigations by TRLFS. J. Colloid Interface Sci. 318 (1), 5–14. https://doi.org/10.1016/j.jcis.2007.09.080.

Tan, X., Fang, M., Wang, X., 2010. Sorption speciation of lanthanides/actinides on minerals by TRLFS, EXAFS and DFT studies: a review. Molecules 15 (11), 8431–8468. https://doi.org/10.3390/molecules15118431.

Texier, A.-C., Andrès, Y., Illemassene, M., Le Cloirec, P., 2000. Characterization of lanthanide ions binding sites in the cell wall of *Pseudomonas aeruginosa*. Environ. Sci. Technol. 34 (4), 610–615. https://doi.org/10.1021/es990668h.

Turgeon, R., Wolf, S., 2009. Phloem transport: cellular pathways and molecular trafficking. Annu. Rev. Plant Biol. 60, 207–221. https://doi.org/10.1146/annurev.arplant.043008.092045.

Tyler, G., 2004. Rare earth elements in soil and plant systems - a review. Plant Soil 267 (1–2), 191–206. https://doi.org/10.1007/s11104-005-4888-2.

Vogel, M., Steudtner, R., Fankhänel, T., Raff, J., Drobot, B., 2021. Spatially resolved Eu (III) environments by chemical microscopy. Analyst 146 (22), 6741–6745. https://doi.org/10.1039/d1an01449h.

Wang, C., Zhu, W., Wang, Z., Guicherit, R., 2000. Rare earth elements and other metals in atmospheric particulate matter in the western part of The Netherlands. Water Air Soil Pollut. 121 (1/4), 109–118. https://doi.org/10.1023/A:1005293131518.

Wen, F., White, G.J., VanEtten, H.D., Xiong, Z., Hawes, M.C., 2009. Extracellular DNA is required for root tip resistance to fungal infection. Plant Physiol. 151 (2), 820–829. https://doi.org/10.1104/pp.109.142067.

White, P.J., 2012. Chapter 3: long-distance transport in the xylem and phloem. In: Marschner's Mineral Nutrition of Higher Plants. Academic Press, pp. 49–70. https://doi.org/10.1016/B978-0-12-384905-2.00003-0.

White, M.C., Baker, F.D., Chaney, R.L., Morris, Decker A., 1981a. Metal complexation in xylem fluid : II. Theoretical equilibrium model and computational computer program. Plant Physiol. 67 (2), 301–310. https://doi.org/10.1104/pp.67.2.301.

White, M.C., Morris, Decker A., Chaney, R.L., 1981b. Metal complexation in xylem fluids: I. Chemical composition of tomato and soybean stem exudate. Plant Physiol. 67, 292–300. https://doi.org/10.1104/pp.67.2.292.

Xu, X., Zhu, W., Wang, Z., Witkamp, G.-J., 2002. Distributions of rare earths and heavy metals in field-grown maize after application of rare earth-containing fertilizer. Sci. Total Environ. 293 (1–3), 97–105. https://doi.org/10.1016/s0048-9697(01)01150-0.

Yang, G., Tan, Q.-G., Zhu, L., Wilkinson, K.J., 2014. The role of complexation and competition in the biouptake of europium by a unicellular alga. Environ. Toxicol. Chem. 33 (11), 2609–2615. https://doi.org/10.1002/etc.2722.

Zha, Z., Wang, D., Hong, W., Liu, L., Zhou, S., Feng, X., Qin, B., Wang, J., Yang, Y., Du, L., Zhang, D., Fang, Z., Xia, C., 2014. Influence of Europium speciation on its

accumulation in *Brassica napus* and *over-expressing BnTR1 lines*. J. Radioanal. Nucl. Chem. 301 (1), 257–262. https://doi.org/10.1007/s10967-014-3120-3.

Zhimang, G., Xiaorong, W., Xueyuan, G., Jing, C., Liansheng, W., Lemei, D., Yijun, C., 2001. Effects of fulvic acid on the bioavailability of rare earth elements and GOT enzyme activity in wheat (*Triticum aestivum*). Chemosphere 44 (4), 545–551. https://doi.org/10.1016/s0045-6535(00)00484-7.

Zhuang, M., Zhao, J., Li, S., Liu, D., Wang, K., Xiao, P., Yu, L., Jiang, Y., Song, J., Zhou, J., Wang, L., Chu, Z., 2017. Concentrations and health risk assessment of rare earth elements in vegetables from mining area in Shandong, China. Chemosphere 168, 578–582. https://doi.org/10.1016/j.chemosphere.2016.11.023.